Engineering Research Express

PAPER

Numerical modeling and analysis of AZO/Cu_2O transparent solar cell with a TiO_2 buffer layer

To cite this article: Naama Sliti *et al* 2023 *Eng. Res. Express* **5** 025013

Engineering Research Express

CrossMark

RECEIVED
18 November 2022

REVISED
3 April 2023

ACCEPTED FOR PUBLICATION
5 April 2023

PUBLISHED
17 April 2023

PAPER

Numerical modeling and analysis of AZO/Cu_2O transparent solar cell with a TiO_2 buffer layer

Naama Sliti[1,2], **Saâd Touihri**[2] and **Ngoc Duy Nguyen**[1]

[1] CESAM | Q-MAT | Solid State Physics, Interfaces and Nanostructures, Institute of Physics B5a, Allée du Six Août 19, B-4000 Liège, Belgium

[2] Ecole Nationale Supérieure d'Ingénieurs de Tunis, Université de Tunis, 13 Ave Taha Hussein, Tunis 1008, Tunis, Tunisia

E-mail: nsi.sliti@uliege.be

Keywords: transparent solar cell, metal oxide, numerical simulation, Cu_2O, TiO_2 buffer layer

Supplementary material for this article is available online

Abstract

In the present work, titanium dioxide (TiO_2) is sandwiched as a buffer layer between n-type aluminum-doped zinc oxide (AZO) and p-type cuprous oxide (Cu_2O), increasing the efficiency of metal oxide-based solar cells. The effects of the device parameters such as thicknesses, carrier concentrations, and defect densities were investigated by numerical simulation to obtain optimal performance of Cu_2O-based solar cells. Our findings reveal that by the incorporation of TiO_2 thin film, the efficiency of the solar cell increases remarkably from 2.54 to 5.02 %. The optimal thicknesses of the Cu_2O and TiO_2 layers are in the range of 10 μm and 0.1 μm, respectively. We obtained optimal photo-electric conversion efficiency of 10.17 % and open-circuit voltage of 1.35 V while achieving 8.90 mA/cm^2 short-circuit current density and 84.12 % fill factor, using structure parameters of 0.2 μm AZO, 0.1 μm TiO_2 and 10 μm Cu_2O with optimal acceptor-type dopant density in Cu_2O of 1E17 cm^{-3} and donor-type dopant density in TiO_2 of 1E18 cm^{-3}.

1. Introduction

Metal-oxide semiconductors have attracted much interest in various applications as they are formed from non-toxic elements that are abundant on Earth and they benefit from good chemical stability and low manufacturing cost [1–3]. Among these oxides, cuprous oxide (Cu_2O) is considered as one of the most promising p-type semiconductor materials, particularly for photovoltaic applications, thanks to its native p-type semi-conductivity, its high majority carrier mobility, and its optical transparency [4–6]. As a result, over the past decade, many Cu_2O-based solar cells that incorporated various n-type semiconductors with large band gap energy, such as aluminum-doped zinc oxide (AZO), have been fabricated with a power conversion efficiency (PCE) between 0.24 % and 3.21 % [7–11]. Despite efforts to fabricate high-performance Cu_2O/AZO heterojunction solar cells, the achieved efficiencies remain significantly lower than the theoretical limit of 20 %, based on the Cu_2O band gap [12]. Additionally, the obtained fill factor and open circuit voltage are also too low. Studies have shown that the main reason for the low efficiency lies in the offset between the conduction band of AZO and Cu_2O [13]. Furthermore, recombination losses at the heterojunction interface can harm solar cell efficiency [14]. Therefore, various buffer layers have been proposed between Cu_2O and AZO layers to reduce interfacial recombination and enhance band alignment across the heterojunction [15–20]. A Cu_2O/AZO-based heterojunction solar cell fabricated with a buffer layer of β-Gallium oxide (Ga_2O_3) was reported by Minami *et al* with an efficiency of 5.38 % [13]. In a recent study, based on one-dimensional simulation and employing 200 μm of Cu_2O supported by different buffer layers, namely ZnO, AGO, and ZnGeO, Naceur *et al* have demonstrated improvements in efficiency from 4.26 to 8.72 % [20]. To build a p-n junction with the p-type Cu_2O layer, an n-type character in the buffer layer is desired. In addition, a wide energy band gap is required to minimize the absorbance of the incident light.

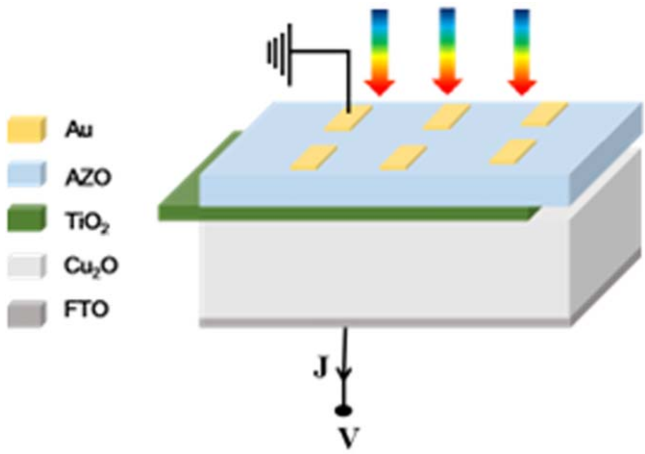

Figure 1. Schematic structure of Cu_2O/AZO solar cell with TiO_2 buffer layer.

A titanium dioxide (TiO_2) thin film can act as a buffer layer in the Cu_2O/AZO structure because of its high optical transparency and good transport properties with a high band gap value of 3 eV [21]. Additionally, TiO_2 can be synthesized in various structures, such as thin films, nanoparticles, and nanorods, that can be synthesized via a wide range of techniques including pulsed-laser deposition [22], sputtering [23], and chemical vapor deposition [24]. The effect of a buffer layer on the characteristics of AZO/Cu_2O thin film solar cells has attracted much interest within the community recently. However, no theoretical or simulation studies have been performed on Cu_2O-based solar cells using a TiO_2 buffer layer. Yet, the importance of device simulation to unveil the relationship between thin film properties and solar cell performance is well established. Moreover, theoretical studies help to explore solar cells with special characteristics at low cost. Such approaches provide a deeper knowledge of the different phenomena that occur in heterojunction solar cells.

In this study, AZO/Cu_2O solar cells without and with a TiO_2 buffer layer are numerically analyzed by the computer simulation software Analysis of Microelectronic and Photonic Structures-1D (AMPS-1D). Aiming at the determination of the device parameters associated with high-performance solar cells, we first analyze the influence of TiO_2 thin film incorporation on the photovoltaic characteristics, like the open-circuit voltage (Voc) and the short-circuit current (Jsc), as well as the cell efficiency and the device fill factor. Subsequently, we determine the optimized values of the device parameters such as layer thickness, doping density, and defect density. The proposed results can contribute to the fundamental knowledge that supports the design and fabrication of solar cells using AZO/Cu_2O heterojunctions.

2. Materials and methods

2.1. Cell structure and material parameters

An illustration of the Cu_2O-based-heterojunction solar cell structure is presented in figure 1. The model contains a p-Cu_2O as an absorber layer as key compound. TiO_2 and AZO n-type thin films were chosen as buffer and window layers, respectively. Table 1 presents the input parameters for each layer in the proposed structure. The front and back contacts of the device are made of fluorine-doped tin oxide (FTO) and gold (Au), respectively. While gold and silver are both commonly used as contact metals, a comparison between the two materials was addressed in the Supplementary data. Gold is preferred as a contact metal due to its large work function, as well as its high conductivity and harmless interfacial reactions [25]. It was assumed that optical reflections at the front contact were negligible. At the front and back contacts, the thermal recombination velocity for holes and electrons was 1.0×10^7 cms^{-1}.

2.2. Numerical modeling

The Analysis of Microelectronic and Photonic Structures (AMPS-1D) software, an effective tool for semiconductor device modeling, was employed to investigate the relationship between the solar cell performance and its physical characteristics [27]. The software provides a detailed analysis of the semiconductor device, and more information on its capabilities can be found in the literature [28–30]. The present work focuses on numerical simulations of AZO/Cu_2O heterojunction solar cells, specifically examining the impact of a TiO_2 buffer layer on the performance of Cu_2O-based solar cells. The study is divided into two parts: the first part analyzes the effect of the buffer layer using physical parameters selected from the literature, while the second part

Table 1. List of input variables from available literature [16, 21, 26].

Parameters	Cu_2O	TiO_2	AZO
Electron affinity [eV]	3.2	3.9	4.4
Thickness [μm]	2–15	0.01–0.1	0.2
Dielectric constant	7.6	10	9
Bang gap [eV]	2.1	3.2	3.35
Shallow uniform donor density [cm^{-3}]	—	5×10^{14}–1×10^{17}	1×10^{21}
Electron mobility [$cm^2 V^{-1} s^{-1}$]	20	100	10
Shallow uniform acceptor density [cm^{-3}]	5×10^{14}–1×10^{17}	—	—
Hole mobility [$cm^2 V^{-1} s^{-1}$]	10	25	5
Effective density of state of VB [cm^{-3}]	2.43×10^{19}	2×10^{17}	1.8×10^{19}
Effective density of state of CB [cm^{-3}]	1.34×10^{19}	6×10^{17}	2.2×10^{18}
Defect type/density [cm^{-3}]	D-like, Gaussian 5×10^{13}–5×10^{15}	D-like, Gaussian 1×10^{15}	D-like, Gaussian 1×10^{18}
Energy level [eV]	Midgap	Midgap	Midgap
Gaussian defect standard deviation	0.1	0.1	0.1
Capture cross section [cm^2]	$5 \times 10^{-13}/1 \times 10^{-15}$	$5 \times 10^{-13}/1 \times 10^{-15}$	$1 \times 10^{-12}/1 \times 10^{-15}$

Table 2. Simulated results for Cu_2O/AZO-based solar cells.

Parameters	J_{SC} [a] [$mA\,cm^{-2}$]	V_{OC} [b] [V]	FF [c] [%]	η [d] [%]
Cu_2O/AZO	7.81	0.65	39.1	2.54
Cu_2O/TiO_2/AZO	8.74	0.84	50.4	5.02

Explanation of symbols in columns
[a] J_{SC}: short circuit current density
[b] V_{OC}: open-circuit potential
[c] FF: fill factor
[d] η: conversion efficiency.

examines the impact of various parameters such as thickness, carrier doping, and defect density on the absorber and buffer layers. As a point of reference, unoptimized Cu_2O/AZO solar cells were employed as a benchmark for evaluation. All simulation calculations were conducted using the AM 1.5 spectrum of illumination (100 $mWcm^{-2}$) and at a temperature of 300 K. The basic semi-classical semiconductor equations, shown here below, including Poisson's equation as well as the current densities derived from the continuity equation, were used for the calculations [31, 32].

$$\frac{d^2}{dx^2}\psi(x) = \frac{e}{\varepsilon_r \varepsilon_0}(p(x) + N_D - n(x) + N_A + \rho_p - \rho_n) \quad (1)$$

$$\frac{dJ_n}{dx} = G - R \quad (2)$$

$$\frac{dJ_p}{dx} = G - R \quad (3)$$

Here Ψ, e, ε_0, and ε_r are the electrostatic potential, the elementary charge, the vacuum permittivity, and the relative permittivity, respectively. The quantities p, n, N_D, N_A, ρ_p, and ρ_n represent the hole concentration, the electron concentration, the donor-type impurity concentration, the acceptor-type impurity concentration, and the holes and electrons distribution. The quantities J_p and J_n present the current density of holes and electrons, while the generation rate and recombination rate are both given by G and R.

3. Results and discussion

The performance of AZO/Cu_2O and AZO/TiO_2/Cu_2O solar cells is examined under AM1.5 illumination and at 300 K. The obtained results are summarized in table 2, based on the settings listed in table 1. The simulated heterojunction solar cell without the TiO_2 buffer layer presents solar output parameters of $V_{oc} = 0.65$ V, $J_{sc} = 7.81$ $mAcm^{-2}$, FF = 39.1 %, and $\eta = 2.54$ %. The obtained efficiency is in accordance with the experimental value of Minami *et al* [13], a reference that we use for comparison and starting point in our study. A considerable improvement is noticed by introducing the TiO_2 intermediate layer between AZO and Cu_2O. As a result, V_{oc}, J_{sc}, FF, and η reached the values of 0.84 V, 8.74 $mAcm^{-2}$, 50.4 %, and 5.02 %, respectively. Figure 2(a) displays the

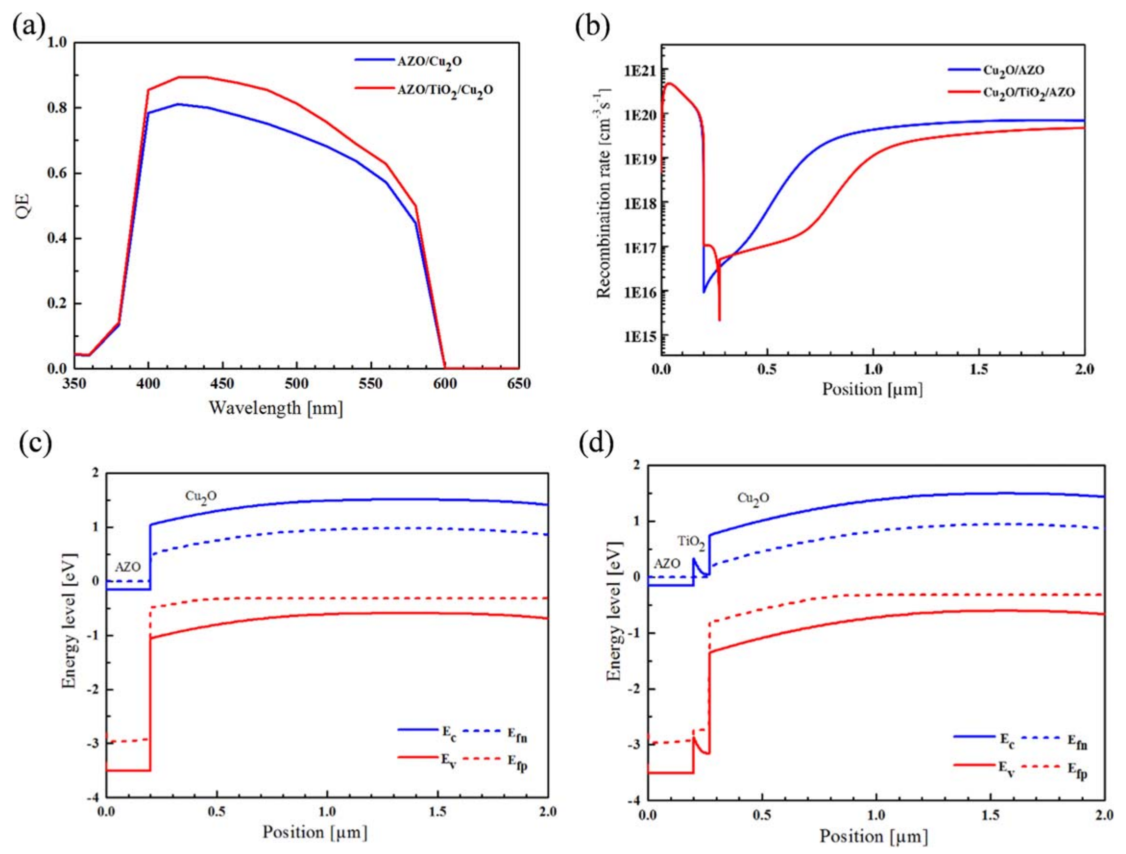

Figure 2. Modeling of Cu_2O-based solar cells: (a) QE, (b) recombination rate distribution, (c) and (d) energy band diagram for AZO/Cu_2O and AZO/TiO_2/Cu_2O heterojunctions at 0 V bias and under illumination, where E_V and E_C represent the maximum of the valence band and the minimum of the conduction band respectively.

quantum efficiency (QE), which increases for the whole spectrum range with the addition of TiO_2 thin film. One should note that the QE edges at ~580 nm and ~400 nm are due to the Cu_2O and AZO materials, which correspond to energy gaps of ~2.1 and ~3.2 eV, respectively [33].

In figure 2(b), it is shown that the TiO_2 buffer layer reduces the recombination rate compared to the structure without it. This result can be related to the selection of minority carriers (electrons) at the TiO_2/Cu_2O interface which reduces the interface recombination. Figures 2(c), (d) shows the energy band diagram of the AZO/Cu_2O junction with a TiO_2 buffer layer having an electron affinity of 3.9 eV. The band diagram shows that the effective value of ΔE_C is reduced with the introduction of the buffer layer from 1.2 to 0.8 eV, which favors the flow of the generated electrons toward the window layer and from there to the electrode [34, 35]. These factors may explain why there is a noticeable improvement between AZO/Cu_2O and AZO/TiO_2/Cu_2O structures, an insight that results directly from the simulations.

Since the AZO/Cu_2O heterojunction solar cell with TiO_2 buffer layer leads to the highest efficiency, we focus hereafter on the impact of a range of absorber parameters including the thickness, doping concentration, and defect density, to provide possible amelioration on the device performance, to optimize the AZO/TiO_2/Cu_2O structure through these parameters.

3.1. Effect of absorber layer parameters on solar cell performances

3.1.1. Cu_2O thickness

In a solar cell, the absorber layer is one of the most fundamental parts. It is crucial to choose the Cu_2O absorber layer thickness appropriately to reduce processing difficulties and increase efficiency. We fix the AZO and TiO_2 thicknesses at 200 nm and 70 nm, respectively, so that we can better understand the effect of Cu_2O thickness. The evolution patterns of the solar cell basic parameters are shown in figure 3, where the Cu_2O thickness varies from 2 to 15 μm. The results show that with the increasing of the Cu_2O thickness from 2 to 10 μm, the values for V_{oc}, J_{sc}, FF, and η do improve. In particular, J_{SC} and η increase rapidly from 8.47 mAcm^{-2} to about 10.38 mAcm^{-2} and from 5.02 % to about 7.98 %, respectively. The open circuit voltage also increases from 0.84 to 1.15 V, which is probably responsible for the fill factor increasing. In fact, the fill factor can be established empirically

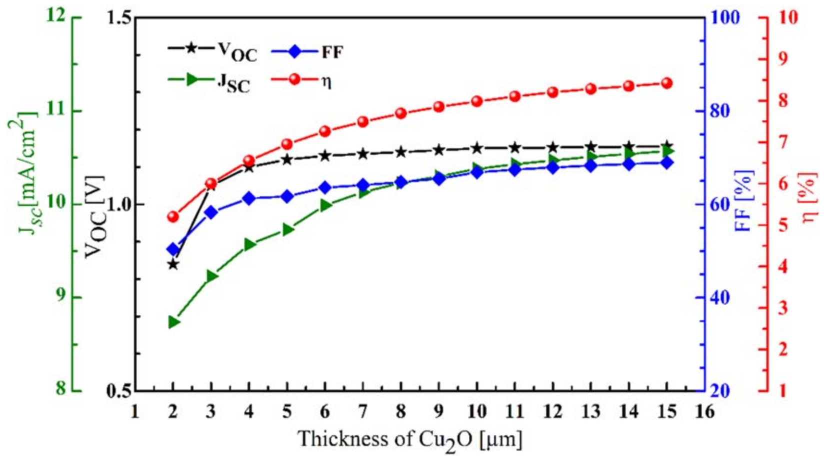

Figure 3. Effect of Cu_2O thickness variation on the Cu_2O-based solar cell output parameters.

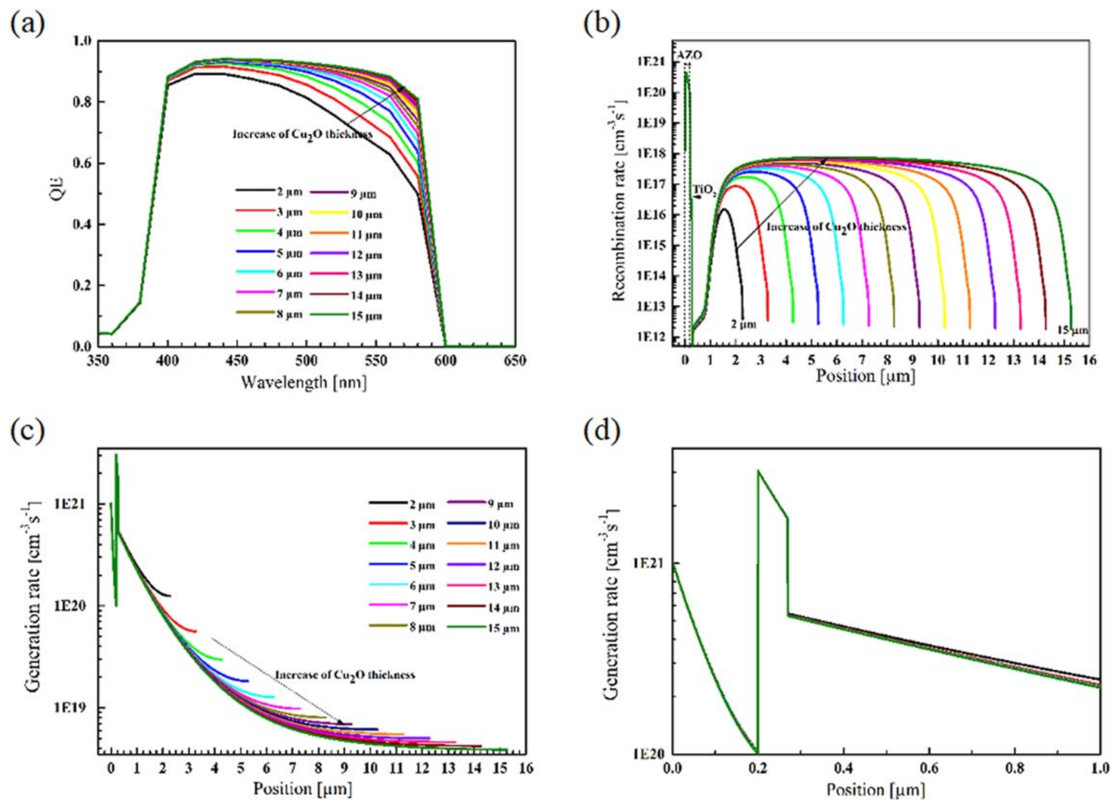

Figure 4. Effect of Cu_2O absorber layer thickness on (a) QE, (b) carrier recombination rate, (c) generation rate, and enlarged view of generation rate of the region between 0 and 1 μm at 0 V bias.

as outlined in [36]. When the absorbent layer of p-Cu_2O is thicker (more than 10 μm), there is almost unchanged in the values of these parameters.

The explanation of such behavior for Cu_2O thickness can be related to the evolution of quantum efficiency. In figure 4(a), the QE increases consistently with increasing Cu_2O layer thickness when the wavelength is between 400 and 600 nm for Cu_2O thicknesses lower than 10 μm. Increasing the thickness of the Cu_2O absorber layer results in the generation of more charge carriers. When the thickness of the Cu_2O film exceeds 10 μm, the QE exhibits little change, which indicates that the cell performances cannot be improved by increasing further the absorber layer thickness. In the ultraviolet region, a small QE results from the absorption of the incident light in the AZO and TiO_2 layers, which leads to charge carrier generation. As a consequence, photo-generated carriers are recombined during the migration process and cannot generate effective QE and there is no

Table 3. Simulated results of solar cells with different doping density N_a of Cu_2O absorber layer.

N_a [cm^{-3}]	5E14	1E15	5E15	1E16	5E16	1E17
V_{OC} [V]	1.15	1.16	1.23	1.26	1.33	1.35
J_{SC} [mA/cm^2]	10.33	10.19	9.8	9.6	9.08	8.85
FF [%]	66.83	70.33	76.72	79.1	82.79	84.38
η [%]	7.94	8.38	9.31	9.64	10.02	10.14

difference in QE value for different Cu_2O thicknesses in this region. The effect of Cu_2O thickness on the efficiency can be also related to the carrier recombination rate and generation rate, as described in figures 4(b) and (c). The carrier generation rates show a similar changing trend, which also reaches a maximum near the Cu_2O/TiO_2 p-n junction and then decreases rapidly for different Cu_2O thicknesses. At the same time, with increasing Cu_2O thickness, the recombination rates of carriers increase in the Cu_2O region.

As a result, the insufficient thickness of the Cu_2O layer cannot fully absorb Sunlight to produce photo-generated carriers, which leads to smaller values of V_{oc}, J_{sc}, η, and QE. So, the increasing thickness of the Cu_2O layer contributes to effectively absorbing incident light and improving solar cell performances. However, an excessive thickness cannot improve solar cell performances and leads to material waste. In this simulation, the proposed optimal thickness of the Cu_2O layer is 10 μm.

3.1.2. Cu_2O doping concentrations

This section aims to study the effect of the Cu_2O doping density (N_a) on the cell parameters. The range of acceptor concentration (N_a) in Cu_2O, according to experimental measurements, is from 1E14 to 1E17 cm^{-3} [37–40]. Simulations were run with N_a values in this range and the thicknesses of Cu_2O, TiO_2, and AZO were set to 10 μm, 70 nm, and 200 nm, respectively.

Table 3 shows that the resulting V_{oc}, η, and FF gradually increase with increasing N_a doping concentration of the Cu_2O layer from 5E14 to 1E17 cm^{-3}. In particular, the efficiency η exhibits an increase from 7.94 to 10.14 %, which means that adjusting the doping density of the Cu_2O layer is an effective way to enhance the efficiency of the solar cell. Meanwhile, the J_{sc} shows a clear decrease from 10.33 to 8.85 mAcm^{-2}. The decrease in J_{sc} is attributed to enhanced carrier recombination, which leads to a decrease in the photo-generated carrier collection [41]. In addition, it is well known that the J_{sc} is related to external quantum efficiency (EQE) and can be calculated via [42]

$$J_{SC} = q \int \Phi(\lambda) EQE(\lambda)\, d\lambda \tag{4}$$

where $\Phi(\lambda)$ represents the spectral photon flux of the AM 1.5 G solar irradiation. From figure 5(a), one observes that the QE exhibits a reduction with the Cu_2O doping concentration increasing.

Figure 5(b) illustrates the variation of carrier recombination rate as a function of doping density in the Cu_2O layer of an $AZO/TiO_2/Cu_2O$ solar cell. The recombination rate decreases in TiO_2 region and increases in Cu_2O region with increasing doping concentration. The energy band diagram (figure 5(c)) explains this effect: higher doping density in Cu_2O layer shifts the conduction and valence band upward, producing a strong electric field (figure 5(d)) that blocks hole flow and reduces interface recombination in TiO_2 region. Furthermore, with increasing doping concentrations, it is obvious that the Fermi level shifts downward to the valence band edge. In this case, the collection of holes on the backside contact electrode (FTO) could be improved. However, high doping of Cu_2O can cause the increase of bulk recombination in the Cu_2O region, leading to a decrease of the QE as well as of J_{sc}. An improvement in V_{oc} and a decrease in J_{sc} are generally associated with the internal electric field in Cu_2O/TiO_2 interface. As a result, an increase in carrier density in the Cu_2O layer can improve the potential barrier at Cu_2O/TiO_2 interface, thereby increasing the performance of Cu_2O solar cells. Therefore, Cu_2O thin films with an acceptor shallow density of 1E17 cm^{-3} will be used in subsequent simulations. This value aligns with reported experimental values for Cu_2O thin films.

3.1.3. Cu_2O Gaussian defect concentrations

Defects in Cu_2O play a crucial role in affecting the performance of devices made from the material. In Cu_2O, the carrier transport occurs through copper and oxygen vacancies (V_{Cu} and V_O) which are prominent defects due to their low formation energies [43]. These defects are modeled with acceptor-like and donor-like Gaussian states, respectively. The copper vacancies (V_{Cu}) generate excess holes, which lead to p-type conduction [44]. Hence, donor-like Gaussian defects were introduced in this simulation. The simulation results for a typical $AZO/TiO_2/Cu_2O$ heterostructure with different donor-like gaussian defects placed in the Cu_2O mid-gap are shown in table 4 and figure 6. These results show that the presence of defects produces harmful effects on the J_{SC}

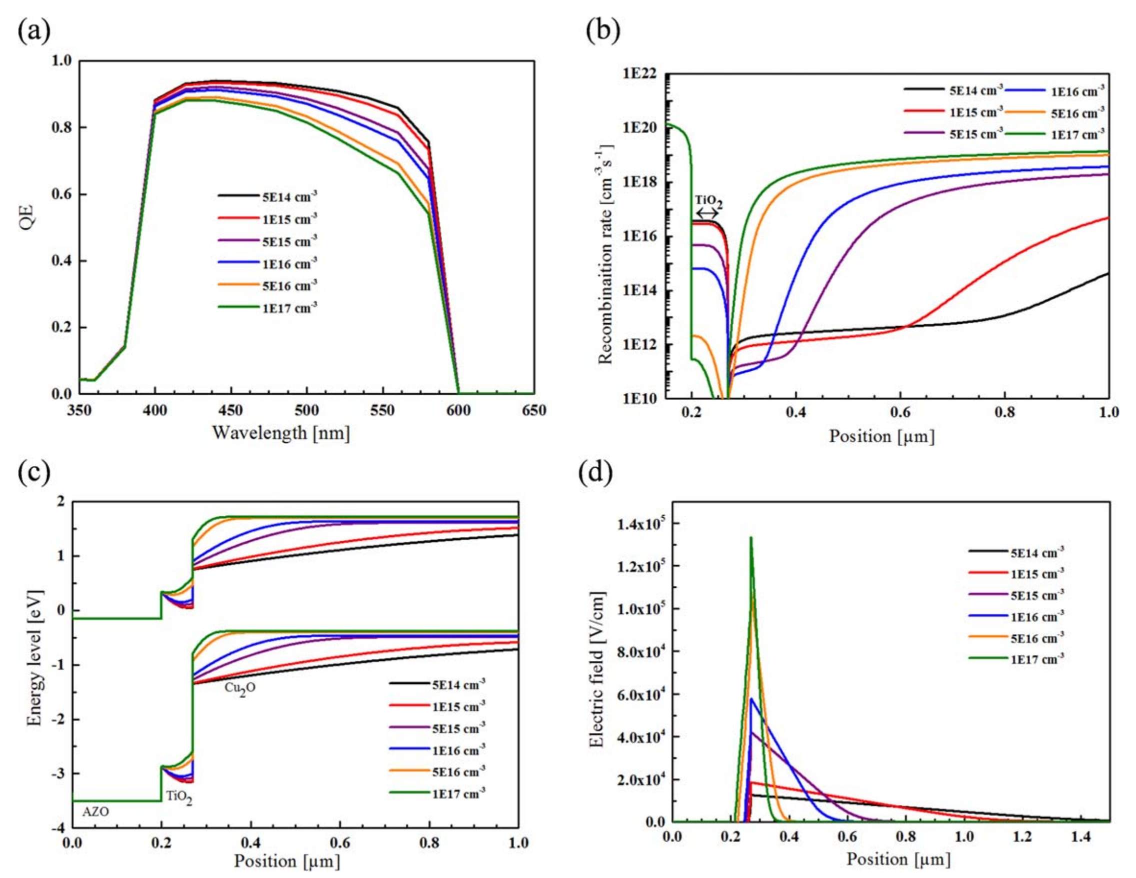

Figure 5. Impact of acceptor doping density in Cu_2O on (a) QE, (b) recombination rate, (c) conduction and valence band alignment, and (d) electric field at 0 V bias and under illumination.

Table 4. Photovoltaic parameters of defective AZO/TiO_2/Cu_2O heterojunction according to defect concentration N_{def} in Cu_2O.

N_{def} [cm^{-3}]	5E13	1E14	5E14	1E15	5E15
V_{OC} [V]	1.35	1.35	1.35	1.35	1.35
J_{SC} [$mAcm^{-2}$]	8.85	8.35	6.97	6.35	5.07
FF [%]	84.38	82.06	77.3	75.89	71.89
η [%]	10.14	9.43	7.51	6.71	5.06

and η values. With the increase in the defect density, the short circuit current shows a decrease from 8.85 to 5.07 $mAcm^{-2}$. It is well known that the bulk defect concentration determines the lifetime of the minority carrier. Excessive defect densities in the Cu_2O layer can act as a center for carrier recombination, leading to a decrease in the photo-generated carrier lifetime and a significant reduction in J_{sc}. This is because the bulk defect concentration determines the lifetime of the minority carrier [45]. Simultaneously, η drops from 10.14 to 5.06 % with the increase of defect density from 5E13 to 5E15 cm^{-3}. Based on these simulation results, we found a good agreement with previous works done in [16] that found a consequential lowering of solar cell performance as defect state density increases in the absorber layer. Thus, controlling the defect concentration in the Cu_2O layer is a critical factor to consider when making heterojunctions.

3.2. Effect of buffer layer parameters on solar cell performances

3.2.1. Buffer layer thickness

Since the TiO_2 layer has the potential to accommodate lattice mismatch and to control the conduction band offset, it is vital to examine the influence of its thickness and doping concentration on solar cell behavior. The thickness of the TiO_2 thin film is varied from 10 to 100 nm while maintaining all other parameters constant. Figure 7(a) shows that J_{sc}, FF, and η increase with increasing TiO_2 thickness while V_{OC} remains constant at a value of about 1.35 V. Moreover, the increase of the TiO_2 thickness from 10 to 100 nm leads to a small increase of η from 9.18 to 10.31 %, which can be correlated by simulation results for QE with the structure that includes the

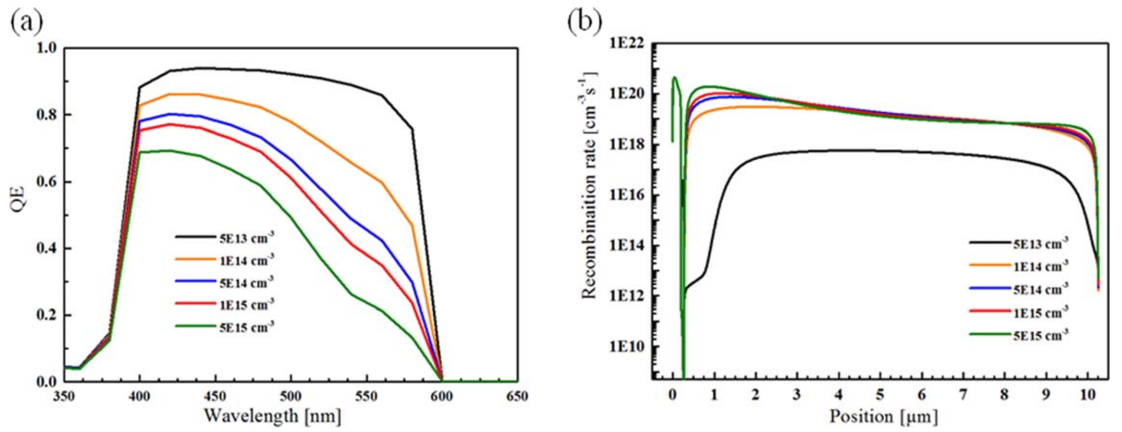

Figure 6. (a) QE and (b) carrier recombination rate as a function of defect density in Cu_2O layer at 0 V bias.

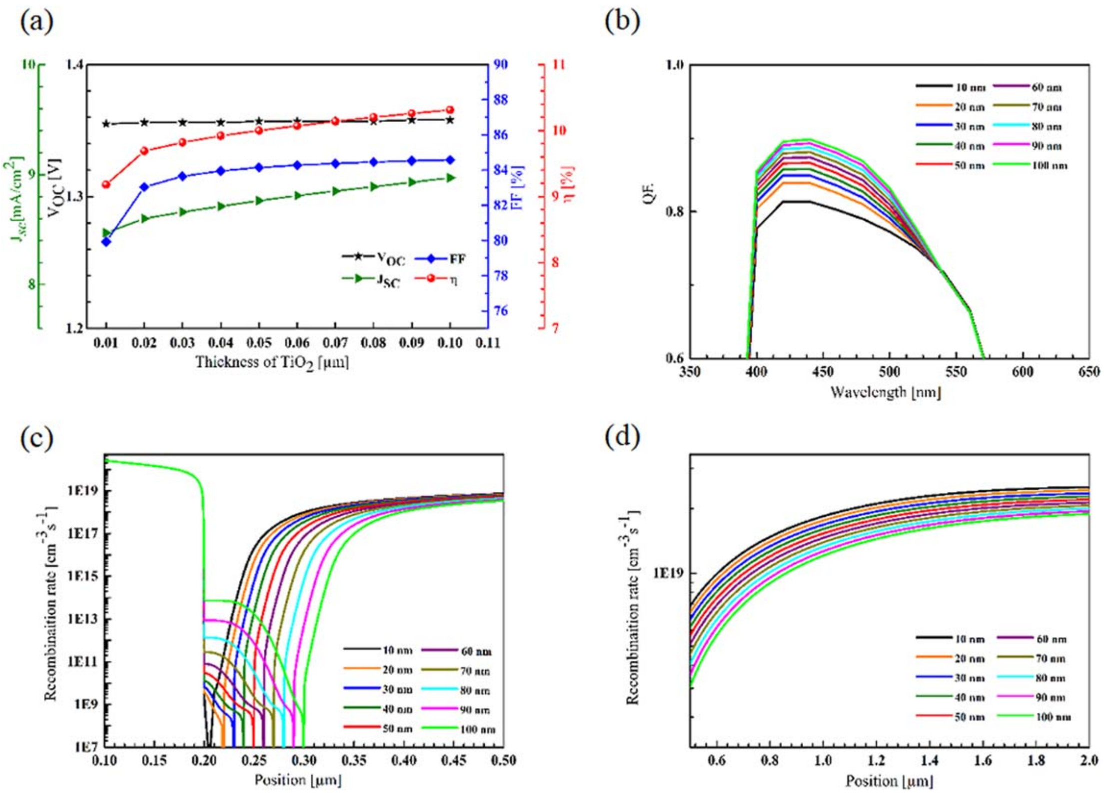

Figure 7. Effect of TiO_2 buffer layer thickness on (a) solar cell parameters (b) QE, (c) carrier recombination rate around the interface junction and (d) recombination rate in Cu_2O region.

TiO_2 buffer layer, as shown in figure 7(b). The impact of the TiO_2 thickness on the recombination rate is shown in figure 7(c). It can be observed that the recombination rate increases in the TiO_2 region, but decreases in the Cu_2O region. This behavior can be interpreted as follows. The TiO_2 layer acts as an electron-selective layer that extracts n-type carriers from the absorber layer. It blocks most of the holes, due to the large offset of the valence band. In addition, it limits the flow of minority carriers from the window layer to the rear surface of the cell. Therefore, as the TiO_2 thickness increases, the recombination rate increases in the TiO_2 region, while decreasing in the Cu_2O region.

3.2.2. Buffer layer (TiO_2) donor concentrations

To explore the influence of the buffer layer doping density on the efficiency of the AZO/TiO_2/Cu_2O heterostructure, the TiO_2 donor concentration was varied from 1E15 to 1E18 cm^{-3}. The results, shown in table 5, reveal that the doping concentration of TiO_2 has only a minor effect on the performance of the proposed

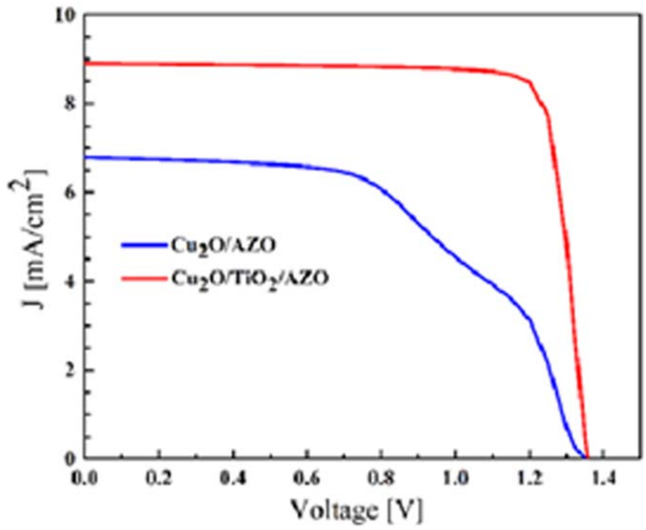

Figure 8. Final J-V curves of AZO/Cu_2O and AZO/TiO_2/Cu_2O transparent solar cells considering the optimized parameters.

Table 5. Simulated results of solar cells with different doping concentrations N_d of TiO_2.

N_d [cm^{-3}]	1E15	1E16	1E17	5E17	1E18
V_{OC} [V]	1.35	1.35	1.35	1.35	1.35
J_{SC} [$mAcm^{-2}$]	8.82	8.82	8.85	8.90	8.90
FF [%]	84.59	84.57	84.38	84.07	84.12
η [%]	10.13	10.13	10.14	10.16	10.17

solar cells. J_{SC} and η show a small increase as N_d increases from 1E15 to 1E18 cm^{-3}, while V_{OC} remains unchanged. It is known that the buffer layer should ideally have a higher n-doping concentration than the absorber layer to enclose the space charge region (SCR) in the last layer. In addition, this configuration should minimize the reverse current by avoiding the generation of minority carriers [29]. The AZO/TiO_2/Cu_2O solar cell performances are consequently relatively unaffected by N_d. As a result, increasing N_d in TiO_2 does not affect the absorption mechanism in the same way as increasing N_a in Cu_2O.

Studying the influence of the TiO_2 layer and optimizing the input parameters of both the buffer and the absorber layers allowed us to tune the device structure to achieve the best performance of a transparent AZO/TiO_2/Cu_2O solar cell. The obtained final J-V curves considering the optimized parameters for AZO/Cu_2O and AZO/TiO_2/Cu_2O solar cells are shown in figure 8. The AZO/TiO_2/Cu_2O device exhibits the highest efficiency value of 10.17 % with the optimum for each parameter, including Cu_2O layer thickness of 10 μm, TiO_2 layer thickness of 0.1 μm, doping concentration N_a of 1E17 cm^{-3} and N_d of 1E18 cm^{-3}, as well as defect concentration in Cu_2O N_{def} 5E13 cm^{-3}. Looking at the effect of heating and of the contact metal work function, the results of which are presented in the Supplementary data, it was found that room-temperature operation and the use of gold are both associated to better performance for the AZO/TiO_2/Cu_2O solar cell. Our results are in line with previous reports in the literature, with Naceur *et al* having reported a PCE of 11.30 % using AZO/ZnGeO/Cu_2O heterojunction solar cell [20]. Our results demonstrate the potential of using non-toxic, Earth-abundant, and sustainable materials in the development of high-performance transparent metal oxide solar cells.

4. Conclusion

In summary, the proposed AZO/TiO_2/Cu_2O heterostructure solar cell was studied through numerical simulations using the AMPS-1D software. We first investigated the role of a TiO_2 buffer layer on the Cu_2O-based heterojunction solar cell characteristics. It was found that the introduction of a TiO_2 thin film improves the efficiency of the solar cell by the reduction of the photogenerated carrier recombination rate and by the enhancement of the band alignment across the heterojunction. Then, to provide an optimization of the input parameters of each layer, the behavior of the solar cell characteristics as a function of layer thickness, doping concentration, and defect density was discussed. Based on the simulation results, optimal thicknesses for Cu_2O and TiO_2 are 10 μm and 100 nm, respectively. Our study also highlights the key role played by the doping concentration and the defect density of Cu_2O. We show that the heterostructure based on a Cu_2O absorber layer with a density of charge carriers value of 1E17 cm^{-3} and defect concentration of 5E13 cm^{-3} delivers promising characteristics. Finally, via the optimization of the TiO_2 doping concentration, we calculated the best values for the cell characteristics: $V_{OC} \sim 1.35$ V, $J_{SC} \sim 8.90$ $mAcm^{-2}$, FF ~ 84.12 %, and $\eta \sim 10.17$ %. These results can serve as relevant indicators for future experimental works aiming at the fabrication of AZO/Cu_2O transparent solar cells with competitive conversion efficiencies.

Acknowledgments

The authors would like to thank Prof *Stephen J Fonash* and his co-worker at the Pennsylvania State University to make available the AMPS-1D program employed in this document.

Data availability statement

The data cannot be made publicly available upon publication because they are not available in a format that is sufficiently accessible or reusable by other researchers. The data that support the findings of this study are available upon reasonable request from the authors.

Author information

Corresponding Author at CESAM | Q-MAT | Solid State Physics, Interfaces and Nanostructures, Physics Institute B5a, Allée du Six Août 19, B-4000 Liège, Belgium.

Funding

The work done by N. S. is partially funded by the Higher National Engineering School of Tunis and by the Académie de recherche et d'enseignement supérieur (ARES, mobility grant). Financial support by the F.R.S-FNRS PINT-MULTI R.8012.20F (INSTEAD Project) is gratefully acknowledged by N. D. N.

ORCID iDs

Naama Sliti https://orcid.org/0000-0002-3183-4054
Saâd Touihri https://orcid.org/0000-0002-6702-9444
Ngoc Duy Nguyen https://orcid.org/0000-0002-0142-1611

References

[1] Selvi K T and Sagadevan S 2022 Recent developments in optoelectronic and photonic applications of metal oxides *Metal Oxides for Optoelectronics and Optics-Based Medical Applications Metal Oxides* ed S Sagadevan *et al* (Amsterdam: Elsevier) pp 33–57
[2] Rühle S, Anderson A Y, Barad H-N, Kupfer B, Bouhadana Y, Rosh-Hodesh E and Zaban A 2012 All-oxide photovoltaics *J. Phys. Chem. Lett.* **3** 3755–64
[3] Wadia C, Alivisatos A P and Kammen D M 2009 Materials availability expands the opportunity for large-scale photovoltaics deployment *Environ. Sci. Technol.* **43** 2072–7
[4] Akimoto K, Ishizuka S, Yanagita M, Nawa Y, Paul G K and Sakurai T 2006 Thin film deposition of Cu_2O and application for solar cells *Sol. Energy* **80** 715–22
[5] Chen L-C 2013 Review of preparation and optoelectronic characteristics of Cu_2O-based solar cells with nanostructure *Mater. Sci. Semicond. Process.* **16** 1172–85
[6] Ghijsen J, Tjeng L H, Van Elp J, Eskes H, Westerink J, Sawatzky G A and Czyzyk M T 1988 Electronic structure of Cu_2O and CuO *Phys. Rev. B* **38** 11322–30
[7] Noda S, Shima H and Akinaga H 2013 Cu_2O/ZnO heterojunction solar cells fabricated by magnetron-sputter deposition method films using sintered ceramics targets *J. Phys. Conf. Ser.* **433** 012027
[8] Sekkat A, Nguyen V H, Masse de la Huerta C, Rapenne L, Bellet D, Kaminski-Cachopo A, Chichignoud G and Muñoz-Rojas D 2021 Open-air printing of Cu_2O thin films with high hole mobility for semitransparent solar harvesters *Commun. Mater.* **2** 1–10
[9] Zhao C, Pan J, Wang B, Dong Z, Jiang Z, Wang J, Song C, Zheng Y and Li C 2018 Photoelectric conversion enhancement of Ag modified p-type Cu_2O/n-type ZnO transparent heterojunction device *J. Mater. Sci., Mater. Electron.* **29** 20485–92
[10] Ievskaya Y, Hoye R L Z, Sadhanala A, Musselman K P and MacManus-Driscoll J L 2015 Fabrication of ZnO/Cu_2O heterojunctions in atmospheric conditions: Improved interface quality and solar cell performance *Sol. Energy Mater. Sol. Cells* **135** 43–8
[11] Miyata T, Watanabe K, Tokunaga H and Minami T 2019 Photovoltaic properties of Cu_2O-based heterojunction solar cells using n-type oxide semiconductor nano thin films prepared by low damage magnetron sputtering method *J. Semicond.* **40** 032701

[12] Meillaud F, Shah A, Droz C, Vallat-Sauvain E and Miazza C 2006 Efficiency limits for single-junction and tandem solar cells *Sol. Energy Mater. Sol. Cells* **90** 2952–9
[13] Minami T, Nishi Y and Miyata T 2013 High-efficiency Cu_2O-based heterojunction solar cells fabricated using a Ga2O3 thin film as N-type layer *Appl. Phys. Express* **6** 044101
[14] Yang T, Liu X, Ding Y, Zhao S and Yin N 2018 Nondestructive interface construction for CdS-buffered ZnO nanorod/Cu_2O composite structure solar cells *J. Nanoparticle Res.* **20** 207
[15] Minami T, Miyata T and Nishi Y 2014 Cu_2O-based heterojunction solar cells with an Al-doped ZnO/oxide semiconductor/thermally oxidized Cu_2O sheet structure *Sol. Energy* **105** 206–17
[16] Fentahun D A, Tyagi A and Kar K K 2021 Numerically investigating the AZO/Cu_2O heterojunction solar cell using ZnO/CdS buffer layer *Optik* **228** 166228
[17] Toghyani Rizi M, Shahrokh Abadi M H and Ghaneii M 2018 Two dimensional modeling of Cu_2O heterojunction solar cells based-on β-Ga_2O_3 buffer *Optik* **155** 121–32
[18] Lahmar H, Azizi A, Schmerber G and Dinia A 2016 Effect of the thickness of the ZnO buffer layer on the properties of electrodeposited p-Cu_2O/n-ZnO/n-AZO heterojunctions *RSC Adv.* **6** 68663–74
[19] Eom K, Lee D, Kim S and Seo H 2018 Modified band alignment effect in ZnO/Cu_2O heterojunction solar cells via Cs_2O buffer insertion *J. Phys. Appl. Phys.* **51** 055101
[20] Naceur K, Tibermacine T, Mehiri F, Boumaaraf R, Labed M, Meftah A, Meftah A and Sengouga N 2021 Study and optimization of Cu_2O/AZO hetero-junction solar cell with different buffer layers *Opt. Mater.* **115** 111060
[21] Sawicka-Chudy P, Sibiński M, Rybak-Wilusz E, Cholewa M, Wisz G and Yavorskyi R 2020 Review of the development of copper oxides with titanium dioxide thin-film solar cells *AIP Adv.* **10** 010701
[22] Ishii A, Nakamura Y, Oikawa I, Kamegawa A and Takamura H 2015 Low-temperature preparation of high-n TiO_2 thin film on glass by pulsed laser deposition *Appl. Surf. Sci.* **347** 528–34
[23] Nezar S, Saoula N, Sali S, Faiz M, Mekki M, Laoufi N A and Tabet N 2017 Properties of TiO2 thin films deposited by rf reactive magnetron sputtering on biased substrates *Appl. Surf. Sci.* **395** 172–9
[24] Shakir S, Abd-ur-Rehman H M, Yunus K, Iwamoto M and Periasamy V 2018 Fabrication of un-doped and magnesium doped TiO2 films by aerosol assisted chemical vapor deposition for dye sensitized solar cells *J. Alloys Compd.* **737** 740–7
[25] Hasan Ali Md S, Islam A T M, Haque M D, Ferdous Rahman Md K, Hossain M, Sultana N and Touhidul Islam A Z M 2023 Numerical analysis of $FeSi_2$ based solar cell with PEDOT:PSS hole transport layer *Mater. Today Commun.* **34** 105387
[26] Chevallier C, Bose S, Hamady S O S and Fressengeas N 2021 Numerical investigations of the impact of buffer germanium composition and low cost fabrication of Cu_2O on AZO/ZnGeO/Cu_2O solar cell performances *EPJ Photovolt.* **12** 3
[27] Liu Y, Sun Y and Rockett A 2012 A new simulation software of solar cells—wxAMPS *Adv. Mater.* **98** 124–8
[28] Boudour S, Bouchama I, Hadjab M and Laidoudi S 2019 Optimization of defected ZnO/Si/Cu_2O heterostructure solar cell *Opt. Mater.* **98** 109433
[29] Oyedele S O and Aka B 2017 Numerical simulation of varied buffer layer of solar cells based on cigs *Model. Numer. Simul. Mater. Sci.* **07** 33
[30] Ying M, Wen J and Zhao Y 2022 Numerical simulation of $CuInSe_2$ solar cells using wxAMPS software *Chin. J. Phys.* **76** 24–34
[31] Abdelfatah M, Ismail W, El-Shafai N M and El-Shaer A 2020 Effect of thickness, bandgap, and carrier concentration on the basic parameters of Cu_2O nanostructures photovoltaics: numerical simulation study *Mater. Technol.* **0** 1–9
[32] Mostefaoui M, Mazari H, Khelifi S, Bouraiou A and Dabou R 2015 Simulation of High efficiency CIGS solar Cells with SCAPS-1D software *Energy Procedia* **74** 736–44
[33] Oku T, Yamada T, Fujimoto K and Akiyama T 2014 Microstructures and photovoltaic properties of Zn(Al)O/Cu_2O-based solar cells prepared by spin-coating and electrodeposition *Coatings* **4** 203–13
[34] Chua D, Kim S B and Gordon R 2019 Enhancement of the open circuit voltage of Cu_2O/Ga_2O_3 heterojunction solar cells through the mitigation of interfacial recombination *AIP Adv.* **9** 055203
[35] Lee Y S, Chua D, Brandt R E, Siah S C, Li J V, Mailoa J P, Lee S W, Gordon R G and Buonassisi T 2014 Atomic layer deposited gallium oxide buffer layer enables 1.2 V open-circuit voltage in cuprous oxide solar cells *Adv. Mater.* **26** 4704–10
[36] Green M A 1981 Solar cell fill factors: general graph and empirical expressions *Solid State Electron.* **24** 788–9
[37] David Prabu R, Valanarasu S, Ganesh V, Shkir M, Kathalingam A and AlFaify S 2018 Effect of spray pressure on optical, electrical and solar cell efficiency of novel Cu_2O thin films *Surf. Coat. Technol.* **347** 164–72
[38] Muñoz-Rojas D, Jordan M, Yeoh C, Marin A T, Kursumovic A, Dunlop L A, Iza D C, Chen A, Wang H and MacManus Driscoll J L 2012 Growth of ∼5 cm2V−1s−1 mobility, p-type Copper(I) oxide (Cu_2O) films by fast atmospheric atomic layer deposition (AALD) at 225 °C and below *AIP Adv.* **2** 042179
[39] Wu H-J, Tomiyama N, Nagai H and Sato M 2019 Fabrication of a p-type Cu_2O thin-film via UV-irradiation of a patternable molecular-precursor film containing Cu(II) complexes *J. Cryst. Growth* **509** 112–7
[40] Sliti N, Fourneau E, Ratz T, Touihri S and Nguyen N D 2022 Mg-doped Cu_2O thin films with enhanced functional properties grown by magnetron sputtering under optimized pressure conditions *Ceram. Int.* **48** 23748–54
[41] Khattak Y H, Baig F, Ullah S, Marí B, Beg S and Ullah H 2018 Numerical modeling baseline for high efficiency (Cu_2FeSnS_4) CFTS based thin film kesterite solar cell *Optik* **164** 547–55
[42] Halme J, Vahermaa P, Miettunen K and Lund P 2010 Device physics of dye solar cells *Adv. Mater.* **22** E210–34
[43] Rajshekar K and Kannadassan D 2021 P-Type Cu_2O thin film transistors for active matrix displays: physical modeling and numerical simulation *IEEE Access* **9** 158842–51
[44] Scanlon D O, Morgan B J, Watson G W and Walsh A 2009 Acceptor levels in p -type Cu_2O : rationalizing theory and experiment *Phys. Rev. Lett.* **103** 096405
[45] Rougieux F, Sun C and Macdonald D 2018 Determining the charge states and capture mechanisms of defects in silicon through accurate recombination analyses: A review *Sol. Energy Mater. Sol. Cells* **187** 263–72